HHS Public Access

Author manuscript

Cancer Res. Author manuscript; available in PMC 2021 August 01.

Published in final edited form as:

Cancer Res. 2021 February 01; 81(3): 634–647. doi:10.1158/0008-5472.CAN-20-1088.

Myeloma-modified adipocytes exhibit metabolic dysfunction and a senescence-associated secretory phenotype (SASP)

Heather Fairfield[1,2,3], **Amel Dudakovic**[4], **Casper M. Khatib**[5], **Mariah Farrell**[1,2,3], **Samantha Costa**[1,2,3], **Carolyne Falank**[1,2,3], **Maja Hinge**[6], **Connor S. Murphy**[1,2,3], **Victoria DeMambro**[1,2,3], **Jessica A. Pettitt**[7], **Christine W. Lary**[1], **Heather E. Driscoll**[8], **Michelle M. McDonald**[7], **Moustapha Kassem**[5,9], **Clifford Rosen**[1,2,3], **Thomas L. Andersen**[10,11], **Andre J. van Wijnen**[4,╪], **Abbas Jafari**[5,*,╪], **Michaela R. Reagan**[1,2,3,*,╪]

[1]Maine Medical Center Research Institute, Scarborough, ME, USA

[2]Tufts University School of Medicine, Boston, MA, USA

[3]University of Maine Graduate School of Biomedical Science and Engineering, Orono, ME, USA

[4]Departments of Orthopedic Surgery and Biochemistry & Molecular Biology, Mayo Clinic, Rochester, MN, USA

[5]Department of Cellular and Molecular Medicine, Novo Nordisk Foundation Center for Stem Cell Biology (DanStem), University of Copenhagen, Copenhagen, Denmark

[6]Department of Internal Medicine, Division of Haematology, Vejle Hospital, Denmark

[7]The Garvan Institute of Medical Research, Sydney, Australia

[8]Department of Biology, Norwich University, Northfield, VT, USA

[9]Molecular Endocrinology & Stem Cell Research Unit (KMEB), Department of Endocrinology and Metabolism, Odense University Hospital & University of Southern Denmark, Odense, Denmark

[10]Clinical Cell Biology, Department of Regional Health Research, Vejle/Lillebaelt Hospital, University of Southern Denmark, Vejle, Denmark

[11]Clinical Cell Biology, Department of Pathology, Odense University Hospital - Department of Clinical Research, University of Southern Denmark, Odense, Denmark

Abstract

Bone marrow adipocytes (BMAd) have recently been implicated in accelerating bone metastatic cancers such as acute myelogenous leukemia and breast cancer. Importantly, bone marrow adipose

[*]**Corresponding authors** Michaela Reagan, 81 Research Drive. Scarborough, ME. 04106, Phone: 1-207-396-8196, mreagan@mmc.org; Abbas Jafari, Mailing: Blegdamsvej 3B, ICMM 18.4.10, DK-2200, Copenhagen N, Denmark. Phone: +45-35337423, ajafari@sund.ku.dk.

╪These last authors share position as co-last authors

Author Contributions: Conception and design (HF, CF, AV, AJ, MR), development of methodology (HF, MH, AV, MR), acquisition of data (HF, AD, CK, SC, CF, MH, VD, JP) analysis and interpretation of data (HF, AD, CK, CF, MF, SC, MH, VD, CL, HD, AV, AJ, CR, MR), writing, review and/or revision of the manuscript (HF and MR wrote the manuscript, all authors contributed to review and revision), administrative (HF, AD, HD, MR), technical (HF, AD, MF, SC, CM,), or material support (MM, TA, MK, AV), study supervision (HF,TA, MM, AV, AJ, MR).

COI: The authors declare no potential conflicts of interest

tissue (BMAT) expands with aging and obesity - two key risk factors in multiple myeloma disease prevalence - suggesting that BMAd may influence and be influenced by myeloma cells in the marrow. Here we provide evidence that reciprocal interactions and cross-regulation of myeloma cells and BMAd play a role in multiple myeloma pathogenesis and treatment response. Bone marrow biopsies from MM patients revealed significant loss of BMAT with myeloma cell infiltration of the marrow, whereas BMAT was restored after treatment for multiple myeloma. Myeloma cells reduced BMAT in different pre-clinical murine models of multiple myeloma and in vitro using myeloma cell-adipocyte co-cultures. In addition, multiple myeloma cells altered adipocyte gene expression and cytokine secretory profiles, which were also associated with bioenergetic changes and induction of a senescent-like phenotype. In vivo, senescence markers were also increased in the bone marrow of tumor-burdened mice. BMAd, in turn, provided resistance to dexamethasone-induced cell cycle arrest and apoptosis, illuminating a new possible driver of myeloma cell evolution in a drug resistant clone. Our findings reveal that bi-directional interactions between BMAd and myeloma cells have significant implications for the pathogenesis and treatment of multiple myeloma. Targeting senescence in the bone marrow adipocyte or other bone marrow cells may represent a novel therapeutic approach for treatment of multiple myeloma.

Keywords

Myeloma; MGUS; adipocytes; senescence; bone marrow; SASP

INTRODUCTION

Multiple myeloma (MM) is a malignant B cell neoplasm characterized by uncontrolled growth of mutated plasma cells within the bone marrow leading to disturbed bone and marrow homeostasis. Overt (symptomatic) myeloma disconnects the normal equilibrium between osteoblastic (bone-building) and osteoclastic (bone-resorbing) activities leading to net bone loss, osteolysis, and pathologic fractures. Properties of the bone marrow allow for migration and proliferation of MM cells, while also providing an environment for quiescent, drug-resistant MM cells (1). Recently, targeting this tumor-supportive microenvironment rather than the cancer cells directly has proven to be an effective and innovative therapeutic strategy to inhibit tumor growth and osteolysis. The effectiveness of this approach is based in part on the pathological manipulation (i.e. hijacking) of the microenvironment by MM cells to create an even more tumor-supportive environment via a positive feedback system (2,3).

The pathogenesis of MM involves complex, bidirectional interactions of MM cells with bone marrow resident cells including osteoblasts, osteoclasts, osteocytes, mesenchymal stem/stromal cells (MSCs), and bone marrow adipocytes (BMAds) (4,5). BMAds have recently been shown to contribute to systemic metabolism via enhanced circulating adipokines (6), and can regulate both bone remodeling via the production of RANKL (7), and hematopoiesis via stem cell factor (SCF) production (8). Interestingly, bone marrow adipose tissue (BMAT) expands with aging and obesity- two key risk factors for myeloma (9)- suggesting that BMAds may contribute to MM disease and progression.

Previously, we demonstrated that myeloma-associated adipocytes exhibit reduced adipogenic gene expression and lipid loss (delipidation) (10), and that adipocytes support MM cell growth (11). Indeed, adipocyte-derived factors such as MCP-1/CCL2 and SDF1α/CXCL12 are chemotactic factors for myeloma cells (4,12), while other adipokines promote myeloma proliferation (e.g. leptin/LEP) (13) and resistance to chemotherapies (e.g. leptin/LEP, adipsin/CFD) (5). In 2019, two main studies examined the relationship between BMAds and myeloma cells, demonstrating that MM-reprogrammed BMAds contribute to myeloma-induced bone disease (14) and that adipocytes are modulated by MM cells in terms of their lipid droplet and adipocyte marker gene expression (15).

Despite these publications, the characteristics of these “MM-modified” adipocytes (MM-adipocytes) remain relatively unexplored and their ability to feedback on tumor cells has not been systematically characterized. In this study, we hypothesized that MM-modified adipocytes regulated MM growth and progression through a secretory profile consistent with senescence. We report an in-depth analysis of MM-adipocytes and detail the ways in which BMAT is altered during myeloma disease progression and treatment, highlighting their unique, tumor supportive phenotypes. Our findings suggest that targeting these MM-adipocytes, or factors derived from them, may represent a new path forward for MM therapy.

MATERIALS AND METHODS

Patient bone marrow biopsies

The control, MGUS and MM cohorts used in this study have been previously described (16,17). All biopsies were collected from Danish pathological biobanks according to the declaration of Helsinki and with approvals by The Regional Scientific Ethical Committees for Southern Denmark (ID S-20070121, S-20110155 and S-20190110). According to these approvals, we were allowed to include diagnostic 3-mm trephine-needle bone marrow biopsies from control, MGUS and MM patients in Danish pathological biobanks without their written informed consent, as long as they had not declined the use of their tissues for research by registering on the National Tissue Application Register. Adjacent 3.5-μm sections from the biopsies were Masson’s trichrome stained or immunostained for CD138 as previously described (16).

Histomorphometry of human biopsies

Adipocyte volume per marrow volume (AV/MV) was estimated as the percentage of points hitting adipocytes versus not in the marrow cavity using the point-grid. An average of 691 (ranging 579–1276) points were evaluated within each biopsy. The adipocyte density was estimated as the number of adipocyte profiles per marrow area (AD density, #/mm^2) within the boxes of the box-grid, and the mean adipocyte profile size (AD size, mm^2) was estimated by measuring the area of the adipocytes profiled within the boxes of the box-grid. The tumor load (MM.Ar/M.Ar) was estimated as the percentage of points hitting $CD138^+$ myeloma cells versus not in the marrow cavity using the point-grid. Quantitation was performed blinded to the clinical data.

Animal experiments

All experimental studies and procedures involving mice were performed in accordance with approved protocols from the Garvan Institute/St. Vincent's Hospital Animal Ethics committee ARA 14/03 (Sydney, Australia) and the Maine Medical Center Research Institute (Scarborough, ME, USA) Institutional Animal Care and Use Committee (IACUC). All mice were weaned at 21 days after birth and fed a diet of normal chow and autoclaved water. Six-week old C57BL/KaLwRiJHsd (BKAL) male mice were injected with vehicle or 5TGM1 cells as described previously (2). In the MM.1S study, 12-week old female Fox Chase SCID-Beige mice (Charles River Laboratory; Wilmington, MA, USA) (n=3–6) were inoculated via tail vein injections with 5×10^6 MM.1S$^{gfp+luc+}$ cells. "Survival endpoints" were euthanasia following MM-induced hind limb paralysis; mice from a predetermined endpoint (21 days following tumor cell inoculation) were used for measuring whole marrow gene expression (n=6). Tumor burden was measured in the MM.1S studies weekly or biweekly utilizing *in vivo* bioluminescence imaging in an IVIS Lumina LT (Perkin Elmer; Waltham, MA) as described previously (18). Following sacrifice, mouse tibia and femora were fixed and stained with hematoxylin and eosin prior to sectioning and imaging as previously described (19).

Cell culture and in vitro *cell functional characterization*

Mouse 3T3-L1 preadipocytes, as well as mesenchymal stromal cells (MSCs) derived from human or mouse bone marrow, or mouse external ears, were cultured and differentiated into adipocytes as described previously (19). MM.1S and 5TGM1 cells were cultured as described (20); OPM-2 and RPMI-8226 cells were similarly grown in RPMI-1640 basal medium supplemented with 10% fetal bovine serum (VWR, Radnor, PA) and 1% penicillin-streptomycin (VWR). For transwell co-culture experiments, preadipocytes or MSCs were seeded into 24- or 6-well plates prior to adipogenic differentiation. Following differentiation, myeloma cells were seeded above mature adipocytes on 0.4 μm transwell membranes (CORNING; Corning, NY). Lipid droplets from adipocytes *in vitro* were labeled with Oil Red O and analyzed (19). For beta-galactosidase staining of senescent cells, differentiated human BMAT samples were exposed to MM cells for 72 hours, then incubated in normal conditions for 10 days, and then fixed and stained for beta-galactosidase (β-gal) using the Senescence β-galactosidase Staining Kit (Cell Signaling Technologies, Danvers, MA) (21). For characterization of myeloma cell phenotypes, cells were collected and stained with APC-Annexin V (Biolegend, San Diego, CA) and DAPI (Thermo Fisher Scientific, Waltham, MA) for apoptosis. For proliferation and cell cycle, cells were fixed in 70% ethanol prior to washing and staining with Alexa Fluor 647 anti-human Ki-67 antibody (Biolegend) and DAPI (0.5 μg/ml) respectively, prior to flow cytometry via MACSQuant Analyzer (Miltenyi Biotec, Bergisch Gladbach, Germany). A minimum of 10,000 events were captured and analyzed using FlowJo v.10 (Becton, Dickinson & Company, Ashland, OR). To compare the effects of MM-BMAT (MM-associated BMAT) and healthy BMAT-derived soluble factors on myeloma cells, conditioned media (CM) was collected from the same BMAT donors (n=7) after 72-hour transwell co-culture experiments (as described above) with/without tumor cells and used with 50/50 fresh media for experiments. For senolytic experiments, BMAT was treated with 500 nM dasatinib (D; Selleck Chemical S1021; Houston, TX, USA) and 100 μM quercetin (Q; Selleck Chemical S2391) for 48

hours approximately 10 days following irradiation (IR) as described (22). BMAT was washed prior to seeding and collection of CM (48h incubation period). Four total BMAT donors were used for IR experiments, with control, non-IR plates paired with IR-plates for each donor.

Total mRNA extraction and quantitative polymerase chain reaction (qPCR)

Total RNA was harvested in QIAZOL and prepared via Qiagen miRNEASY Kit with DNase On-column digestion (Qiagen; Hildnen, Germany) according to the manufacturer's protocol. RNA was quantified and tested for quality and contamination using a Nanodrop 2000 (Thermo Fisher Scientific) and subjected to quality control minimum standards of 260/230>2 and 260/280>1.8 prior to downstream applications. qPCR was executed as previously described (19).

Microarray gene expression analysis

Total RNA (100 ng) from 3T3-L1 cells was used for cRNA synthesis, prepared and purified as described (20). Briefly, 5.5 μg of fragmented single-strand cDNA (GeneChip ® WT PLUS reagent Kit) was purified, labeled and hybridized prior to injection into Mouse Clariom S arrays. Arrays were placed in the Affymetrix® GeneChip® Hybridization Oven 645, and stained with the Affymetrix GeneChip Fluidics Station 450 prior to scanning (7G Affymetrix GeneChip Scanner 3000). Raw data (Affymetrix CEL files) were imported into the Gene Expression Workflow (Partek Genomics Suite v. 6.17.0918, Partek, St Louis, MO) (GSE143269) and normalized prior to log2 transformation, and differential expression (DE) analysis, as previously described (20), except here a one-way ANOVA was utilized in the DE analysis and DE genes were defined based on an absolute fold change (FC)>1.5 in combination with an unadjusted p-value ≤ 0.05.

Protein assessment in adipocyte conditioned media and cell lysates

Cell culture conditioned media (CM) was collected from mature naïve adipocytes or MM-adipocytes in culture and frozen at −20°C. Secreted cytokines in the CM were quantified with either the Mouse Adipokine Array (R&D) or the Human Cytokine Array (R&D; Minneapolis, MN) per the manufacturer's instructions. 3T3-L1 IL-6 protein secretion was also measured using a mouse-specific IL-6 ELISA (R&D) with or without MM.1S co-culture (direct or indirect (using a 0.4μm transwell)).

Mitochondrial respiratory function analysis

A Seahorse XF Cell Mito Stress Test kit was run utilizing a Seahorse XFe96 analyzer (Agilent Technologies, Santa Clara, CA). 3T3-L1 cells were seeded in a 96-well Seahorse XF cell culture microplate density of 5×10^3 cells/well and adipogenesis was induced. At day 7 of differentiation, cells were transferred to maintenance media with either 50% MM-CM or basal media for 3 days, and on day 10, the test was run according to manufacturer instructions.

RNA-Sequencing of human BMAT and MM cell co-cultures

High throughput RNA-Sequencing (RNA-Seq) was performed on human BMAT, differentiated from human MSCs from three donors, and three human MM cell lines. BMAT from each donor was either cultured alone or exposed to one of the three human MM cell lines via transwell co-culture for 72 hours. Similarly, each MM cell line was cultured alone or exposed to one of three BMAT donors prior to RNA collection and purification as outlined above. RNA libraries were prepared and high-throughput read mapping and bioinformatics analyses were executed as described (23) (GSE140374).

Analysis of External Primary Plasma Cell Data set from GEO

Gene expression data were downloaded from the Gene Expression Omnibus (GSE6477) (24), log-transformed, and analyzed with a one-way ANOVA model using the aov() function in R. Heatmaps were generated using the heatmap.2() function in R.

Cell line validation

Data generated from RNA-Seq was used to validate the MM.1S, OPM-2, and RPMI-8226 cells. Base-calling and variant determination was performed using Illumina's RTA version 1.17.21.3, and the MAPRSeq bioinformatics pipeline (http://bioinformaticstools.mayo.edu/research/maprseq) as described (23). Variants were compared to RNA-Seq variants present in the Cancer Cell Line Encyclopedia (portals.broadinstitute.org/ccle; (25)) utilizing publicly available tools from Galaxy (use.galaxy.org). Known translocations were confirmed using gene fusion predictions resulting from the MAPRSeq pipeline, and also compared against CCLE gene fusion predictions. 3T3-L1 cells were from ATCC (www.atcc.org). 5TGM1 cells have not been validated at this time.

Cell Line	Source	Cell Authentication	Mycoplasma Test	Number of Passages
MM.1S $^{gfp+luc+}$	Ghobrial Laboratory, 2015	RNA-Seq Variant Analysis	2015	1–30
5TGM1 $^{gfp+luc+}$	Ghobrial Laboratory, 2015	N/A	2015	1–30
RPMI-8226	Ghobrial Laboratory, 2015	RNA-Seq Variant Analysis	2017	1–30
OPM-2^{luc+}	Ghobrial Laboratory, 2015	RNA-Seq Variant Analysis	2015	1–30
3T3-L1	ATCC	N/A (ATCC)	N/A	1–10

Statistical Analysis

All graphs were created with GraphPad Prism (version 5 or 7); statistical significance was determined using one-way or two-way ANOVA, or Student's T-Test unless otherwise stated. Non-linear regression using Gaussian model with Least squares fitting method was used to present and compare bone marrow adipocyte size distribution profiles. Data represent mean ± SEM unless otherwise noted. Significance is indicated as: *, $p<0.05$; **, $p<0.01$; ***, $p<0.001$; ****, $p<0.0001$.

Additional Methods details can be found in the supplementary information.

RESULTS

Myeloma cells decrease BMAT in MM patients and murine myeloma models

To gain insight into the relationship between BMAds and myeloma cells, we explored BMAT changes in bone marrow from newly-diagnosed MM patients. Iliac crest biopsies from MM patients contained a large number of BMAds, many of which were flanked by $CD138^+$ myeloma cells (Fig. 1A), suggesting bidirectional signaling between these cells. Quantification of BMAds indicated a significant decrease in adipocyte volume fraction (adipocyte volume per marrow volume, AV/MV) (Fig. 1B) and mean adipocyte size (Fig. 1C), as well as significantly altered adipocyte size profiles (Supp. Fig. 1A) in newly-diagnosed MM patient samples compared to controls, but no change in adipocyte density (Fig. 1D). Interestingly, the reduced adipocyte volume fraction and size in MM samples was independent of the tumor load in the BM, indicating that decreased BMAT in MM is not simply due to crowding of the marrow by MM cells (Fig. 1E–G). Interestingly, treatment of MM increased the adipocyte volume fraction (Fig. 1H) and density (Fig. 1J) in patients. Moreover, we observed significant alteration of the adipocyte size distribution profile after treatment, mainly due to increased frequency of medium-sized adipocytes, and decreased frequency of larger or smaller adipocytes (Supp. Fig. 1B), such that the mean adipocyte size was unchanged (Fig. 1I). Thus, BMAT is altered in MM patients based on treatment or stage of disease.

To model what occurs in patients and explore the BMAT-MM relationship more deeply, we next examined the bone marrow of C57BL/KaLwRij (BKAL) mice harboring $5TGM1^{gfp+luc+}$ MM cells (Fig. 2A) (2). Histological analysis of femurs harvested 21 days after tail vein injection of MM cells (Fig. 2B,C) indicated that bone marrow adiposity was decreased in terms of AV/MV (Fig. 2D) and adipocyte density (Fig. 2F), but not adipocyte size (Fig. 2E). Furthermore, bone marrow adiposity was not correlated with tumor burden as assessed via bone marrow GFP^+ flow cytometry (2). We next employed a SCID-Beige human xenograft bone-homing $MM.1S^{gfp+luc+}$ mouse model (18) (Fig. 2G; femoral H&E images Fig. 2H,I). $MM.1S^{gfp+luc+}$ proliferation *in vivo* was confirmed via luciferase activity at 14, 17 and 21 days post-injection (Fig. 2J). Histological analysis of femurs harvested at the terminal endpoint (determined by hind-limb paralysis), indicated presence of a large number of BMAds in proximal femurs of control animals (Fig. 2H), which were largely absent in tumor-bearing mice (Fig. 2I). Quantification of BMAds revealed that MM.1S-bearing mice had significantly decreased AV/MV (Fig. 2K), BMA size (Fig. 2L) and density (Fig. 2M). Overall, BMAT in MM mouse models and human MM patient samples was decreased, demonstrating that MM infiltration alters BMAds, a phenomenon observed across mammalian species that may contribute to disease progression.

Myeloma reduces adipocyte lipid content and induces widespread gene expression changes in mouse adipocytes

We next characterized how MM cells affect BMAds using *in vitro* co-cultures. We first utilized 3T3-L1 adipocytes to increase reproducibility of our results by eliminating the

potential confounding effects of a mixed stromal population or donor variability present in primary samples. 3T3-L1 pre-adipocytes were differentiated into adipocytes and exposed to myeloma cells via indirect transwell co-culture for 72 hours (Fig. 3A). 3T3-L1 adipocytes exposed to MM.1S cells had decreased lipid content (Fig. 3B) and significantly reduced expression of the early adipogenic transcription factor *Cebpa*, as well as mature adipocyte genes *Adipoq* and *Fabp4,* when co-cultured with MM.1S or 5TGM1 cells (Fig. 3C). Similarly, 3T3-L1 adipocytes exposed to MM-conditioned media (MM-CM) had reduced lipid content (Supp. Fig. 2A) and adipogenic gene expression (Supp. Fig. 2B). Furthermore, primary adipocytes derived from mouse bone marrow MSCs (Fig. 3D) and mouse ear MSCs (Supp. Fig. 2C) co-cultured with MM cells using transwells also exhibited reduced adipogenic mRNA transcripts. Hence, MM cells suppress normal adipogenic functions in differentiated adipocytes.

Microarray analysis of 3T3-L1 adipocytes with or without transwell co-culture with MM.1S cells revealed 71 differentially expressed genes (Fig. 3E, Supp. Table 1). In total, 28 genes were significantly downregulated (FC<−1.5), and 43 genes were upregulated (FC>1.5) in the adipocytes co-cultured with MM cells. Pathway-ANOVA analysis of significantly altered transcripts indicated that MM cells affect vital cellular pathways and significantly alter Oxidative phosphorylation and cellular processes (eg. Ribosome, Cytokine-cytokine receptor interactions, Cell cycle, and Spliceosome) (Table 1). These transcriptome changes reflect the loss of the adipogenic phenotype in 3T3-L1 cells.

Myeloma cells induce aberrant gene expression in human BMAds including decreased adipogenic and increased senescence-associated transcripts

We next investigated the relationship between BMAT and myeloma cells utilizing RNA sequencing (RNA-Seq). Human MSCs from three similarly-aged donors were differentiated into BMAT and then co-cultured with or without MM cells (MM.1S, OPM-2, or RPMI-8226) for 72 hours using transwells. RNA-Seq revealed significant changes in BMAT gene expression profiles in response to MM (MM-BMAT), and many of these genes were tightly connected with nodes and grouped into functions, as evidenced by STRING-db (Fig. 4A) and GeneMania analyses (Supp. Fig. 3A,B). The largest significant increase was found to be in the gene podoplanin (*PDPN)*, a gene also expressed in other cancer-associated adipocytes (26), and cancer-associated fibroblasts (CAFs) (27), where its expression levels predicts less favorable clinical outcomes (28).

BMAT exposed to MM.1S cells (BMAT_MM.1S) exhibited the greatest response (number of genes with large expression fold changes), followed by BMAT exposed to OPM2 (BMAT_OPM2) and then BMAT exposed to RPMI-8226 (Supp. Fig. 3C). 102 significantly upregulated genes were common to all three MM-associated BMAT samples; these fell into KEGG pathways including “Pathways in Cancer”, “Proteoglycans in Cancer” and “Cellular Senescence” (Supp. Table 2). Indeed, when genes encoding senescence-associated secretory phenotype (SASP) (29) proteins were examined in MM-BMAT, compared to BMAT alone, many were upregulated including: *SERPINB2* (204x), *IL6* (175x), *ICAM1* (33x), *CXCL1* (58x), *CXCL2* (39x), and *VEGFA* (5x) (Fig. 4B). These results suggest that myeloma cells induce senescence in adipocytes, with genes encoding SASP proteins (eg. *IL6, IL8, CXCL1,*

and CXCL2) among the top 10 genes increased in response to MM.1S and OPM-2 cell lines individually (Supp. Table 3). The top 10 up- and downregulated genes in BMAT in response to each MM cell line are shown in Supplemental Tables 3 and 4 respectively. Importantly, MM.1S and OPM-2 significantly induced *IL6* expression in BMAT (Supp. Table 3), while no *IL6* expression was observed in the myeloma cells themselves- either basally or after exposure to BMAT.

Only a few genes (16) were commonly downregulated in response to myeloma (Supp. Fig. 3D; Supp. Table 4), but all 3 MM cell lines appeared to decrease important processes in BMAT, such as *Metabolism* and *Signaling by Receptor Tyrosine Kinases* (Supp. Table 5), according to pathway analysis of RNA-Seq data. In agreement with our previous *in vitro* data, BMAT also exhibited marked reduction in adipogenic transcripts in response to MM cell co-culture (Fig. 4B). A noteworthy decrease across MM-BMAT (Supp. Fig. 3E) was phosphoinositide-3-kinase regulatory subunit 3 (*PIK3R3*/p55; red box), which interacts with PPARγ/*PPARG* to increase adipogenesis, while dominant negative p55 inhibits adipogenesis (30). *SOX18* was the most downregulated molecule in MM-BMAT (Supp. Fig. 3F), decreased on average approximately 4-fold. These changes suggest MM-associated BMAT is indeed distinct from healthy BMAT, and likely plays a unique functional role in influencing myeloma cells.

Myeloma cells induce a senescence-like phenotype and abnormal metabolism in adipocytes

To validate that MM cells functionally induce a SASP in BMAds, we conducted 72 hour indirect co-cultures utilizing 5 additional bone marrow donors and MM.1S cells. Human MSC-derived BMAT was exposed to MM.1S cells for 72 hours, and then fixed and stained for the senescence marker β-galactosidase (β-gal) (21). Significantly fewer lipid-containing adipocytes were identified in the co-culture versus controls and the majority of MM-associated adipocytes at this time point were β-gal positive (Supp. Fig. 4A, B; Fig. 4C). We also confirmed highly elevated expression levels of four SASP genes: *IL6* (Fig. 4D), *CSF2* (Supp. Fig. 4C), *CXCL1* (Supp. Fig. 4D), and *CXCL2* (Fig. 4E), in response to MM.1S and OPM-2 via qPCR and observed slight increases in the protein secretion of the SASP proteins IL-6, IL-8, and CCL2/MCP1 in MM-BMAT (Fig. 4F). To test whether senescence can occur *in vivo*, we examined SASP gene expression in whole bone marrow samples from SCID-Beige mice. We detected elevated *Il-6* (Supp. Fig. 4E) and *Cxcl1* (Supp. Fig. 4F) expression in MM.1S tumor bearing mice compared to naïve mice 21 days after tumor cell injection. In a study by Liu et al., BMAds isolated from MM patients in complete remission were shown to exhibit reduced adipogenesis (14); we re-analyzed this publicly available data utilizing GEO2R and found that these adipocytes also exhibit marked increases in the SASP gene signature (29) (Supp. Fig. 4G), although not all results reached significance due to a small sample size. To explore IL-6 protein changes in MM-adipocytes, we co-cultured 3T3-L1 adipocytes with MM.1S cells or alone and measured IL-6 secretion into the CMs of these cultures by mouse-specific ELISA. 3T3-L1 adipocytes exposed to MM.1S cells exhibited increased IL-6 secretion after only 4 hours in direct co-culture (MM D), and significant increases in both direct and indirect (MM ID) transwell co-culture systems at 24 and 48 hours (Fig. 5A). 72-hour exposure to MM.1S-CM also increased IL-6 secretion in these

adipocytes and revealed significant increases in other cytokines including the melanocortin receptor antagonist Agouti-related neuropeptide (AgRP/*Agrp*), Lipocalin-2 (*Lcn2*), RAGE/*Ager*, RANTES/*Ccl5*, and RBP4/Rbp4, and reduced IGF-2/*Igf2* (Fig. 5B).

Because senescent cells often have altered metabolisms, and our RNA-seq, microarray, and prior data suggested aberrations in MM-BMAT metabolism, we performed bioenergetic studies using the Seahorse XF Cell Mito Stress Test on 3T3-L1 adipocytes exposed to MM-CM (Fig. 5C). MM-CM-treated adipocytes exhibited significant increases in basal oxygen consumption rates (OCR) (Fig. 5D) and non-mitochondrial respiration (Fig. 5E), the latter being indicative of increased ROS generation which damages mitochondria. Furthermore, MM-CM-treated cells exhibited trends towards increased proton leak (Fig. 5F) further indicating damage from increased oxidative stress (31). These damaged mitochondria result in metabolically dysfunctional cells, requiring higher levels of ATP for maintaining organelle integrity, resulting in the increased basal OCR noted above (32). Taken together, these results suggest that MM-CM-treatment is damaging to the mitochondria of adipocytes such that they produce an aberrant cytokine profile, which includes elevated release of IL-6, a cytokine known to support myeloma cells *in vitro* and *in vivo*.

Specific signals from myeloma cells may induce the MM-BMAT phenotype

We next interrogated our RNA-seq data for common, highly-expressed genes in the 3 MM cell lines that could explain their ability to induce senescence in BMAT. Under normal maintenance conditions, the three MM cell lines expressed 10,662 common, highly-expressed genes (Supp. Fig. 5A) including *HMGB1* and *HMGB2* (Supp. Fig. 5B). These two soluble proteins can trigger NF-κB (*NFKB1*) and P38/MAPK pathways (which were increased in MM-BMAT, Supp. Table 2) to initiate the production of IL-6/*IL6* (33) or directly modulate chromatin opening at SASP gene loci (34). Interestingly, *HMGB3* was also increased in 3T3-L1 adipocytes exposed to MM cells (Fig. 3E). Thus, although we cannot be certain which proteins from MM cells induce the senescent phenotype in BMAds, our data suggest that the HMGB family may be involved.

We then investigated how MM cells alter adipogenesis. Our analysis of publicly available data (24) found that the expression of adipogenesis regulators is altered in myeloma cells (Supp. Fig. 6A,B). Notably, the gene expression levels of *WNT5A*, *TGFB1*, and *TNF* (Supp. Fig. 6A; orange arrows), which encode secreted, soluble negative regulators of adipocyte differentiation (Supp. Fig. 6C), are elevated in all stages of myeloma disease: MGUS, Smoldering, Overt, and Relapsed (Supp. Fig. 6A). Indeed, all three of our cell lines exhibit basal expression of one or more of these genes (Supp. Fig. 6D), suggesting that these proteins are likely factoring into the reduced adipogenesis of MM-BMAds.

The three MM cell lines used in our study exhibited vastly different expression profile changes (Supp. Fig. 7A–C) in response to adipocytes, reflecting their distinct biological origins from different donors and subsequent adaptation to culture in different laboratories. Yet, six genes were commonly upregulated (>2x) among all three lines (Fig. 6A; Supp. Fig. 8A) and no genes were commonly downregulated (>2x; Supp. Fig. 8B). The upregulated genes (Supp. Fig. 8C) were analyzed with STRING analysis, (Fig. 6A; Supp. Fig. 7 red boxes) and 3 of these (*KLF9*, *TSC22D3*, and *FKBP5*) are implicated in glucocorticoid

receptor signaling (35). Increased expression of *FKBP5* (Fig. 6B), *KLF9* (Fig. 6C), and *PARP9* (Supp. Fig. 8D) was confirmed in MM.1S and OPM-2 lines co-cultured with three BMAT donors via qPCR. Hence, irrespective of major distinctions in transcriptomes of different MM cell lines, there is a select number of upregulated genes that may contribute to pro-survival effects of adipocytes on MM cells.

BMAds are implicated in supporting MM cell resistance to therapy in vitro *and clinically*

To explore if the observed changes in glucocorticoid receptor signaling-related transcripts translated to differences in dexamethasone (dex) responsiveness, we co-cultured MM.1S in transwell with human MSC-derived BMAT and examined apoptosis, proliferation, and cell cycle with or without dex. When exposed to dex, MM.1S cells exhibited a nearly 3-fold increase in total apoptosis, which was severely diminished when co-cultured with BMAT (Fig. 6D). Similarly, the dex-induced reduction in proliferation, as measured by the percent of Ki67 ($MKI67^{+}$ cells, was also rescued by BMAT co-culture (Fig. 6E). Dex also altered MM.1S progression through cell cycle (Supp. Fig. 8E); however in the presence of BMAT, the percent of MM.1S cells in sub G1 was partially rescued and a complete rescue of S phase populations was observed (Fig. 6F). To investigate the clinical relevance of these findings, we next examined BMAT in MM patient iliac crest biopsies prior to their treatment with high-dose melphalan and dexamethasone followed by autologous bone marrow transplantation. Interestingly, we found that individuals who showed a complete response to treatment had significantly lower BMAT volume fraction (AV/MV) before treatment (−54%, $P<0.05$) compared to patients with partial/very good partial response (Fig. 6G). These findings support our *in vitro* data, suggesting that higher BMAT prior to treatment protects MM cells against chemotherapy. Thus, interactions between MM cells and adipocytes protect MM cells against the apoptotic effects of dex and add a new layer to the “vicious cycle” of myeloma progression.

Next, to clearly delineate effects of MM-BMAT vs naïve BMAT, which is difficult in transwell co-cultures, we tested conditioned media from MM-BMAT (BMAT that had been co-cultured in transwell with MM.1S cells for 72 hours) and naïve BMAT from matched donors for their effects on MM cells (Fig. 6H). MM.1S cells exhibited a significant ~40% decrease in cell number in response to dexamethasone alone. Naïve BMAT CM elicited a proliferative effect on MM cell number, as well as dexamethasone resistance. Conversely, MM-BMAT CM induced was a slight, non-significant decrease in MM cell number but, similar to naïve BMAT CM, also induced dex resistance. The dex resistance induced by naïve or MM-BMAT was similar (Supp. Fig 8F).

Finally, we created senescent human BMAT *in vitro* by administering 10Gy irradiation to differentiated BMAT and evaluated its effects on MM cells. We also investigated whether senescent BMAT could be targeted by senolytics (dasatinib and quercetin (D+Q), Supp. Fig. 9A, B). CMs from these samples were applied to MM.1S cells. Similar to MM-BMAT CM, we observed a significant reduction in MM cell number in response to IR BMAT, but not control BMAT, (Supp. Fig. 9B) suggesting that senescent BMAT differentially effects MM cells. We also observed dex resistance in MM cells treated with CM from IR BMAT (but not control BMAT). These data suggest that IR BMAT may induce a drug resistant and

potentially more dormant phenotype in MM cells. Importantly, in CM collected from IR BMAT following treatment with D+Q for 48 hours, we observed increased sensitivity to dex, and no restoration of MM cell numbers. Collectively, these data indicate novel functions of BMAT in MM and suggest that healthy and senescent (myeloma-associated or irradiated) BMAT provide resistance to MM treatment (Fig. 6I), although potentially through different mechanisms.

DISCUSSION

Our study demonstrates that MM cells disrupt the normal bone marrow microenvironment by decreasing adiposity and inducing a SASP in BMAds. These observations are observed in both patient-derived samples and murine models, reflecting conservation of the pathological mechanism in mammalian species. Our patient data demonstrate no direct correlation between bone marrow tumor burden and bone marrow adiposity in overt MM, arguing against a “space-constricted” mechanism causing decreased BMAT. The mechanism of decreased marrow adiposity varied between our patient data and *in vivo* models, demonstrating the need for multiple methods of interrogating BMAT response to tumor cells. Overall, these data support the interpretation that MM cells inhibit bone marrow adiposity in mice and humans, and induce senescence in BMAds. Hence, senescent BMAds may be a new biological target for senolytic strategies to treat MM, which may be even more relevant clinically since aging is a major MGUS and MM risk factor.

One of the hallmarks of cancer-associated senescent cells is the presence of a SASP, which involves the secretion of molecules used by cancer cells to promote their growth and survival. Senescence in tumor-related stromal cells has been observed in myeloma patient MSCs and other cancer-associated cells (3,36–38). Senescent cells also contribute to age-related bone loss (39). Importantly, we observed increases in adipocyte *IL6*/IL-6 and *IL8*/CXCL1 gene expression and secreted protein in adipocytes upon MM co-culture. These findings were recapitulated in whole bone marrow samples from tumor-bearing mice compared to naïve controls, providing *in vivo* evidence of a myeloma-driven SASP phenotype. Moreover, other CXCL family members were also upregulated in MM-adipocytes, such as *CXCL5*, *CXCL6*, and *CXCL7*. Although these CXCL members are not considered typical senescence-related chemokines, these ligands can bind the same CXCR2 receptor as known SASP proteins CXCL1, CXCL2, and CXCL3 (40). Upregulation of these senescence-associated genes strengthens the emerging concept that MM-BMAds are senescent, and supports the notion that MM-BMAT inflammatory SASP proteins contribute to myeloma progression or related bone disease. Indeed, Liu and colleagues recently reported that MM-adipocytes release soluble factors that inhibit osteoblastogenesis and stimulate osteoclastogenesis (14). Reduced levels of adiponectin (*ADIPOQ*), adipsin (*CFD*) and visfatin (*NAMPT*), as well as increased TNFα (*TNF*) in MM-adipocytes contributed to this imbalance. Our reanalysis of the data (14) demonstrated increases of other SASP-related transcripts (Supp. Fig. 4E), which could also contribute to MM bone disease. Ozcan and colleagues investigated the relationship between senescent MSCs and myeloma cells *in vitro* and observed a substantial effect on myeloma cell cycle and proliferation in co-cultures, and differences in effects between naïve cells and myeloma “primed” or pre-exposed cells (41). These findings demonstrate that myeloma cell proliferation is modulated by senescence-

related factors, and that myeloma cells may reprogram neighboring cells to support their survival. Overall, our findings integrate well with data suggesting that myeloma induces senescence in the marrow, and that this may further contribute to MM disease.

We also observed that MM cells consistently suppressed *Pparg/PPARG* and other adipokines in adipocytes. It has been reported that MM-BMAds have reduced PPARγ signaling (14) and that reprogramming by MM cells occurs with direct contact via integrin-α6, despite the fact that identical changes were observed with indirect contact, although to a lesser extent. Our data argue that indirect (CM and transwell) co-culture, not via integrin signaling, is also sufficient to induce this PPARγ/*PPARG* change in MM-BMAds. Our study suggests that, in addition to basal expression of *WNT5A*, *TGFB1*, and *TNF*, high *HMGB1* and *HMGB2* expression by myeloma cells contributes to this MM-associated adipocyte phenotype. HMGB1 signals via toll-like receptor 4 (TLR4) to trigger NF-κB and P38/MAPK pathways, activating the production of IL-6/*IL6* and MCP1/*CCL2* in adipocytes (33). Myeloma-derived HMGB1 may elicit similar effects from BMAds, as both the TLR4 cascade and NF-κB signaling pathway were both significantly upregulated in the MM-associated adipocyte dataset. HMGB2 is also highly expressed in myeloma cells, and has been shown to regulate SASP gene expression by aiding in chromatin opening at SASP gene loci (34). Thus, high HMGB1 and HMGB2 expression may contribute to the MM-associated adipocyte phenotype. Cell-line specific expression differences including high expression of *S100A4* (42) in RPMI-8226, *IL-32* (43) in OPM-2, and *CCL3* (44) in MM.1S, have also been shown to modulate expression of either adipogenic genes or inflammatory factors, and may modulate the MM-adipocyte phenotype. Together, this complex cocktail of MM cell secreted signaling molecules contributes to the MM-adipocyte phenotype by suppressing metabolism and driving a senescent phenotype.

Despite advances in myeloma treatment, patients continue to develop drug resistance and relapse, in part due to interactions between MM cells and microenvironmental cells\, such as pre-adipocytes and adipocytes (4). Mouse preadipocyte CM can enhance myeloma chemotaxis via activation of the Wnt signaling cascade, while mature adipocyte CM can promote myeloma growth through the ERK signaling cascade (4). Similarly, human adipocyte CM confers increased viability (by increased STAT-3) to myeloma cells and stimulates angiogenesis *in vitro* (12). BMAd-derived leptin and adipsin also support myeloma cell chemotherapy resistance through the induction of autophagy and subsequent reduction of apoptosis (5). While these mechanisms may be involved in the dexamethasone resistance reported here, we also demonstrate downregulation of these adipokines in MM-BMAds, and specific increases in the genes known to be involved in glucocorticoid receptor trafficking in co-cultured MM cells. Thus, our findings reveal previously under-appreciated driving mechanisms through which BMAds support MM disease progression.

We also observed consistently increased expression of poly(ADP-ribose) polymerase family member 9 (*PARP9*) in all three MM cell lines in response to BMAT co-culture. *PARP9*, also known as B-aggressive lymphoma or (BAL/BAL1), is highly expressed in high risk diffuse large B-cell lymphomas (45) and breast cancer (46), and can promote migration in these cancer cells. PARP9 stimulates phosphorylation of STAT1 to ultimately suppress p53 via IRF1, thereby enhancing proliferation and reducing apoptosis (47), two phenotypes that we

observed in our MM cells cultures with BMAds when challenged with dexamethasone. Thus, while we demonstrated upregulation of genes intimately involved in glucocorticoid receptor trafficking and subsequent dexamethasone resistance, BMAT also induces expression of other survival pathways (Supp. Fig. 7; MAPK/BCL2, Negative Regulation of Apoptosis, JAK/STAT Signaling, Interferon Signaling) which may be related to PARP9; this will be investigated in future studies.

In MM.1S cells, we observed significant increases in cells in S-phase and dexamethasone resistance, when co-cultured with MM-BMAT in transwells (Fig. 6D–F). We also observed that CM from naïve BMAT increased MM cell numbers while MM-BMAT CM decreased cell numbers (Fig 6H), while both CM types induced dex resistance, suggesting that MM-BMAT supports tumor cells by mechanisms distinct from healthy BMAT. Irradiated BMAT was similar to MM-BMAT in that both decreased MM cell numbers over time (suggesting dormancy in tumor cells) while inducing dexamethasone resistance. It is possible that senescent BMAT induces a dormant or senescent phenotype in MM cells, as suggest with a potential S-phase arrest in MM cells in transwell co-culture with BMAT, although other factors may also be at play. Interestingly, senescence can be induced in cells from nearby senescent cells, which may be occurring here (41). This potential phenomenon and the potential for dormancy-driven drug resistance to be occurring in MM cells necessitate further investigation. Future directions should also compare BMAds induced to undergo senescence through different mechanisms (eg. aging, irradiation, or culture with MM cells), and assess differences their effects on MM cells.

In terms of translational relevancy, irradiated BMAT treated with senolytics (D+Q) restored sensitivity to dexamethasone and resulted in the lowest tumor cell number after 72 hour treatment. Combined, these results suggest that senescent and senescent-like adipocytes support dexamethasone resistance, and that this can be partially rescued with senolytic treatment. Targeting senescent BMAs may reflect a new therapeutic option for targeting microenvironment-induced drug resistance in myeloma without inducing proliferation of MM cells. (As an aside, BMAT used to make CM for experiments in Supp. Fig 9B and Fig. 6H were from different donors and cultured for different times, due to different requirements for the irradiation protocol; these differences likely explain differences in the BMAT-CM effects observed. This highlights that within each experiment, the same BMAT donors should always be used, and as many primary human samples should be used as possible, to capture human donor variability).

In conclusion, our studies demonstrate that BMAT changes dramatically in murine myeloma models and human patients. Adipocytes exposed to myeloma-derived factors exhibited decreased lipid content, decreased adipogenic transcripts, and increased expression of SASP transcripts and proteins including *IL6*/IL-6. Signals from MM-adipocytes affected myeloma cell number, response to dexamethasone, cell cycle states, and expression of genes related to glucocorticoid receptor signaling, which could affect the availability of the glucocorticoid receptor for ligand binding and nuclear localization (48–50). Senescent, MM-BMAT, and naïve BMAT have different effects on MM cells, and all contribute to dexamethasone resistance. Lastly, it is plausible that SASP proteins from MM-associated BMAds contribute to the vicious cycle of MM-induced osteolysis, beyond other established functions such as

autocrine inhibition of adipogenesis and generating a tumor-supportive microniche (14). Therefore, removal of these cells via senolytic therapies could have a two-fold benefit of alleviating bone damage and diminishing myeloma drug resistance.

Supplementary Material

Refer to Web version on PubMed Central for supplementary material.

ACKNOWLEDGEMENTS

We thank Drs. Calvin Vary and Anyonya Guntur for their intellectual contributions, Dr. Anne Breggia and the Maine Medical Center Biobank, and Dr. Asha Nair from Biomedical Statistics and Informatics Core at Mayo Clinic. We also thank the caregivers taking care of the authors' children so the authors could perform this work. Funding: This work was supported by the American Cancer Society (Research Grant #IRG-16-191-33 and RSG-19-037-01-LIB), the NIH (R24 DK092759-01, U54GM115516, R01AR049069, R37CA245330, and P20GM121301), the Danish Southern Region Research Grant (20/14282; Andersen PI), and the Kane Foundation. Microarray and functional analysis were supported by the Vermont Biomedical Research Network (VBRN) Bioinformatics Core, which is supported by an Institutional Development Award (IDeA) from the National Institute of General Medical Sciences of the National Institutes of Health under grant number P20GM103449.

Financial Support: This work was supported by funds awarded to Dr. Reagan including start-up funds from the Maine Medical Center Research Institute, Metabolics COBRE (NIH/NIGMS P20GM121301; Liaw PI) a pilot project from the American Cancer Society (Research Grant #IRG-16-191-33; Reagan PI), an American Cancer Society Research Scholar Grant (RSG-19-037-01-LIB), the NIH/NIDDK (R24 DK092759-01), the Kane Foundation, and a grant from the National Cancer Institute (R37CA245330). Microarray data collection and analysis was supported by the Vermont Genetics Network Microarray and Bioinformatics Core facilities through Grant #P20GM103449 from the INBRE program of the NIGMS/NIH. Additional support was provided by NIH/NIAMS (R01 AR049069) and The Danish Southern Region Research Grant (20/14282; Andersen PI).

REFERENCES

1. Reagan MR, Liaw L, Rosen CJ, Ghobrial IM. Dynamic Interplay between Bone and Multiple Myeloma: Emerging Roles of the Osteoblast. Bone. 2015;75:161–9. [PubMed: 25725265]
2. McDonald MM, Reagan MR, Youlten SE, Mohanty ST, Seckinger A, Terry RL, et al. Inhibiting the osteocyte-specific protein sclerostin increases bone mass and fracture resistance in multiple myeloma. Blood. 2017;129:3452–64. [PubMed: 28515094]
3. Reagan MR, Mishima Y, Glavey SV, Zhang YY, Manier S, Lu ZN, et al. Investigating osteogenic differentiation in multiple myeloma using a novel 3D bone marrow niche model. Blood. 2014;124:3250–9. [PubMed: 25205118]
4. Trotter TN, Gibson JT, Sherpa TL, Gowda PS, Peker D, Yang Y. Adipocyte-Lineage Cells Support Growth and Dissemination of Multiple Myeloma in Bone. Am J Pathol. 2016;186:3054–63. [PubMed: 27648615]
5. Liu Z, Xu J, He J, Liu H, Lin P, Wan X, et al. Mature adipocytes in bone marrow protect myeloma cells against chemotherapy through autophagy activation. Oncotarget. 2015;6:34329–41. [PubMed: 26455377]
6. Fowler JA, Lwin ST, Drake MT, Edwards JR, Kyle RA, Mundy GR, et al. Host-derived adiponectin is tumor-suppressive and a novel therapeutic target for multiple myeloma and the associated bone disease. Blood. 2011;118:5872–82. [PubMed: 21908434]
7. Fan Y, Hanai J, Le PT, Bi R, Maridas D, DeMambro V, et al. Parathyroid Hormone Directs Bone Marrow Mesenchymal Cell Fate. Cell Metab. 2017;25:661–72. [PubMed: 28162969]
8. Boyd AL, Reid JC, Salci KR, Aslostovar L, Benoit YD, Shapovalova Z, et al. Acute myeloid leukaemia disrupts endogenous myelo-erythropoiesis by compromising the adipocyte bone marrow niche. Nat Cell Biol. 2017;19:1336–47. [PubMed: 29035359]
9. Marinac CR, Suppan CA, Giovannucci E, Song M, Kværner AS, Townsend MK, et al. Elucidating Under-Studied Aspects of the Link Between Obesity and Multiple Myeloma: Weight Pattern, Body

Shape Trajectory, and Body Fat Distribution. JNCI cancer Spectr. 2019;3:pkz044. [PubMed: 31448358]

10. Fairfield H, Harris EJ, Falank C, Reagan MR. Myeloma-Associated Adipocytes Exhibit Reduced Adipogenic Gene Expression and Delipidation. Blood. 2017;130:1768. [PubMed: 28827411]
11. Falank C, Fairfield H, Farrell M, Reagan MR. New Bone Cell Type Identified As Driver of Drug Resistance in Multiple Myeloma: The Bone Marrow Adipocyte. Blood. 2017;130:122.
12. Bullwinkle EM, Parker MD, Bonan NF, Falkenberg LG, Davison SP, DeCicco-Skinner KL. Adipocytes contribute to the growth and progression of multiple myeloma: Unraveling obesity related differences in adipocyte signaling. Cancer Lett. 2016;380:114–21. [PubMed: 27317873]
13. Caers J, Deleu S, Belaid Z, De Raeve H, Van Valckenborgh E, De Bruyne E, et al. Neighboring adipocytes participate in the bone marrow microenvironment of multiple myeloma cells. Leukemia. 2007;21:1580–4. [PubMed: 17377589]
14. Liu H, He J, Koh SP, Zhong Y, Liu Z, Wang Z, et al. Reprogrammed marrow adipocytes contribute to myeloma-induced bone disease. Sci Transl Med. 2019;11:eaau9087. [PubMed: 31142679]
15. Morris EV, Suchacki KJ, Hocking J, Cartwright R, Sowman A, Gamez B, et al. Myeloma Cells Down-Regulate Adiponectin in Bone Marrow Adipocytes Via TNF-Alpha. J Bone Miner Res. John Wiley and Sons Inc.; 2019;
16. Hinge M, Delaisse J-M, Plesner T, Clasen-Linde E, Salomo M, Andersen TL. High-dose therapy improves the bone remodelling compartment canopy coverage and bone formation in multiple myeloma. Br J Haematol. 2015;171:355–65. [PubMed: 26212720]
17. Abdelgawad ME, Delaisse J-M, Hinge M, Jensen PR, Alnaimi RW, Rolighed L, et al. Early reversal cells in adult human bone remodeling: osteoblastic nature, catabolic functions and interactions with osteoclasts. Histochem Cell Biol. 2016;145:603–15. [PubMed: 26860863]
18. Natoni A, Farrell ML, Harris S, Falank C, Kirkham-McCarthy L, Macauley MS, et al. Sialyltransferase inhibition leads to inhibition of tumor cell interactions with E-selectin, VCAM1, and MADCAM1, and improves survival in a human multiple myeloma mouse model. Haematologica. 2019;haematol.2018.212266.
19. Fairfield H, Falank C, Harris E, Demambro V, McDonald M, Pettitt JAJ, et al. The skeletal cell-derived molecule sclerostin drives bone marrow adipogenesis. J Cell Physiol. 2017;233:1156–67. [PubMed: 28460416]
20. Fairfield H, Falank C, Farrell M, Vary C, Boucher JM, Driscoll H, et al. Development of a 3D bone marrow adipose tissue model. Bone. 2018;1:77–88.
21. Noren Hooten N, Evans MK. Techniques to Induce and Quantify Cellular Senescence. J Vis Exp 2017;
22. Zhu Y, Tchkonia T, Pirtskhalava T, Gower AC, Ding H, Giorgadze N, et al. The Achilles' heel of senescent cells: from transcriptome to senolytic drugs. Aging Cell. 2015;14:644–58. [PubMed: 25754370]
23. Dudakovic A, Camilleri E, Riester SM, Lewallen EA, Kvasha S, Chen X, et al. High-resolution molecular validation of self-renewal and spontaneous differentiation in clinical-grade adipose-tissue derived human mesenchymal stem cells. J Cell Biochem. NIH Public Access; 2014;115:1816–28. [PubMed: 24905804]
24. Chng WJ, Kumar S, Vanwier S, Ahmann G, Price-Troska T, Henderson K, et al. Molecular dissection of hyperdiploid multiple myeloma by gene expression profiling. Cancer Res. 2007;67:2982–9. [PubMed: 17409404]
25. Ghandi M, Huang FW, Jané-Valbuena J, Kryukov GV., Lo CC, McDonald ER, et al. Next-generation characterization of the Cancer Cell Line Encyclopedia. Nature. Nature Publishing Group; 2019;569:503–8.
26. Trevellin E, Scarpa M, Carraro A, Lunardi F, Kotsafti A, Porzionato A, et al. Esophageal adenocarcinoma and obesity: peritumoral adipose tissue plays a role in lymph node invasion. Oncotarget. Impact Journals; 2015;6:11203–15.
27. Kumcu E, Unverdi H, Kaymaz E, Oral O, Turkbey D, Hucmenoglu S. Stromal podoplanin expression and its clinicopathological role in breast carcinoma. Malays J Pathol. 2018;40:137–42. [PubMed: 30173230]

28. Hu G, Wang S, Xu F, Ding Q, Chen W, Zhong K, et al. Tumor-Infiltrating Podoplanin+ Fibroblasts Predict Worse Outcome in Solid Tumors. Cell Physiol Biochem. 2018;51:1041–50. [PubMed: 30476924]
29. Coppé J-P, Patil CK, Rodier F, Sun Y, Muñoz DP, Goldstein J, et al. Senescence-associated secretory phenotypes reveal cell-nonautonomous functions of oncogenic RAS and the p53 tumor suppressor. Downward J, editor. PLoS Biol. 2008;6:2853–68. [PubMed: 19053174]
30. Iankova I, Petersen RK, Annicotte J-S, Chavey C, Hansen JB, Kratchmarova I, et al. Peroxisome Proliferator-Activated Receptor γ Recruits the Positive Transcription Elongation Factor b Complex to Activate Transcription and Promote Adipogenesis. Mol Endocrinol. 2006;20:1494–505. [PubMed: 16484339]
31. Avila C, Huang R, Stevens M, Aponte A, Tripodi D, Kim K, et al. Platelet Mitochondrial Dysfunction is Evident in Type 2 Diabetes in Association with Modifications of Mitochondrial Anti-Oxidant Stress Proteins. Exp Clin Endocrinol Diabetes. 2012;120:248–51. [PubMed: 21922457]
32. Chacko BK, Kramer PA, Ravi S, Benavides GA, Mitchell T, Dranka BP, et al. The Bioenergetic Health Index: a new concept in mitochondrial translational research. Clin. Sci. (Lond). 2014 page 367–73.
33. Gunasekaran MK, Virama-Latchoumy A-L, Girard A-C, Planesse C, Guérin-Dubourg A, Ottosson L, et al. TLR4-dependant pro-inflammatory effects of HMGB1 on human adipocyte. Adipocyte. 2016;5:384–8. [PubMed: 27994953]
34. Aird KM, Iwasaki O, Kossenkov AV., Tanizawa H, Fatkhutdinov N, Bitler BG, et al. HMGB2 orchestrates the chromatin landscape of senescence-associated secretory phenotype gene loci. J Cell Biol. 2016;215:325–34. [PubMed: 27799366]
35. Rees-Unwin KS, Craven RA, Davenport E, Hanrahan S, Totty NF, Dring AM, et al. Proteomic evaluation of pathways associated with dexamethasone-mediated apoptosis and resistance in multiple myeloma. Br J Haematol. 2007;139:559–67. [PubMed: 17979943]
36. André T, Meuleman N, Stamatopoulos B, De Bruyn C, Pieters K, Bron D, et al. Evidences of Early Senescence in Multiple Myeloma Bone Marrow Mesenchymal Stromal Cells. PLoS One. 2013;8:e59756. [PubMed: 23555770]
37. Alameda D, Saez B, Lara-Astiaso D, Sarvide S, Lasa M, Alignani D, et al. Characterization of freshly isolated mesenchymal stromal cells from healthy and multiple myeloma bone marrow: transcriptional modulation of the microenvironment. Haematologica. Ferrata Storti Foundation (Haematologica); 2020;haematol.2019.235135.
38. Prime SS, Cirillo N, Hassona Y, Lambert DW, Paterson IC, Mellone M, et al. Fibroblast activation and senescence in oral cancer. J. Oral Pathol. Med Blackwell Publishing Ltd; 2017 page 82–8. [PubMed: 27237745]
39. Farr JN, Xu M, Weivoda MM, Monroe DG, Fraser DG, Onken JL, et al. Targeting cellular senescence prevents age-related bone loss in mice. Nat Med. 2017;23:1072–9. [PubMed: 28825716]
40. Acosta JC, Gil J. A role for CXCR2 in senescence, but what about in cancer? Cancer Res. 2009 page 2167–70. [PubMed: 19276354]
41. Özcan S, Alessio N, Acar MB, Toprak G, Gönen ZB, Peluso G, et al. Myeloma cells can corrupt senescent mesenchymal stromal cells and impair their anti-tumor activity. Oncotarget. 2015;6:39482–92. [PubMed: 26498687]
42. Hou S, Jiao Y, Yuan Q, Zhai J, Tian T, Sun K, et al. S100A4 protects mice from high-fat diet-induced obesity and inflammation. Lab Investig. 2018;98:1025–38. [PubMed: 29789685]
43. Lin X, Yang L, Wang G, Zi F, Yan H, Guo X, et al. Interleukin-32α promotes the proliferation of multiple myeloma cells by inducing production of IL-6 in bone marrow stromal cells. Oncotarget Impact Journals, LLC; 2017;8:92841–54. [PubMed: 29190960]
44. Gerhardt CC, Romero IA, Cancello R, Camoin L, Strosberg AD. Chemokines control fat accumulation and leptin secretion by cultured human adipocytes. Mol Cell Endocrinol. Elsevier; 2001;175:81–92. [PubMed: 11325518]

45. Aguiar RCT, Yakushijin Y, Kharbanda S, Salgia R, Fletcher JA, Shipp MA. BAL is a novel risk-related gene in diffuse large B-cell lymphomas that enhances cellular migration. Blood. 2000;96:4328–34. [PubMed: 11110709]

46. Tang X, Zhang H, Long Y, Hua H, Jiang Y, Jing J. PARP9 is overexpressed in human breast cancer and promotes cancer cell migration. Oncol Lett Spandidos Publications; 2018;16:4073–7. [PubMed: 30128030]

47. Camicia R, Bachmann SB, Winkler HC, Beer M, Tinguely M, Haralambieva E, et al. BAL1/ARTD9 represses the anti-proliferative and pro-apoptotic IFN -STAT1-IRF1-p53 axis in diffuse large B-cell lymphoma. J Cell Sci. 2013;126:1969–80. [PubMed: 23487038]

48. Urashima M, Teoh G, Chauhan D, Hoshi Y, Ogata A, Treon SP, et al. Interleukin-6 overcomes p21WAF1 upregulation and G1 growth arrest induced by dexamethasone and interferon-gamma in multiple myeloma cells. Blood. 1997;90:279–89. [PubMed: 9207463]

49. Cai B, Wang S, Huang J, Lee C-K, Gao C, Liu B. Cladribine and bendamustine exhibit inhibitory activity in dexamethasone-sensitive and -resistant multiple myeloma cells. Am J Transl Res. e-Century Publishing Corporation; 2013;5:36–46. [PubMed: 23390564]

50. Hsu S, DeFranco DB. Selectivity of Cell Cycle Regulation of Glucocorticoid Receptor Function. J Biol Chem. 1995;270:3359–64. [PubMed: 7852422]

Statement of Significance:

This study changes the foundational understanding of how cancer cells hijack the bone marrow microenvironment and demonstrates that tumor cells induce senescence and metabolic changes in adipocytes, potentially driving new therapeutic directions.

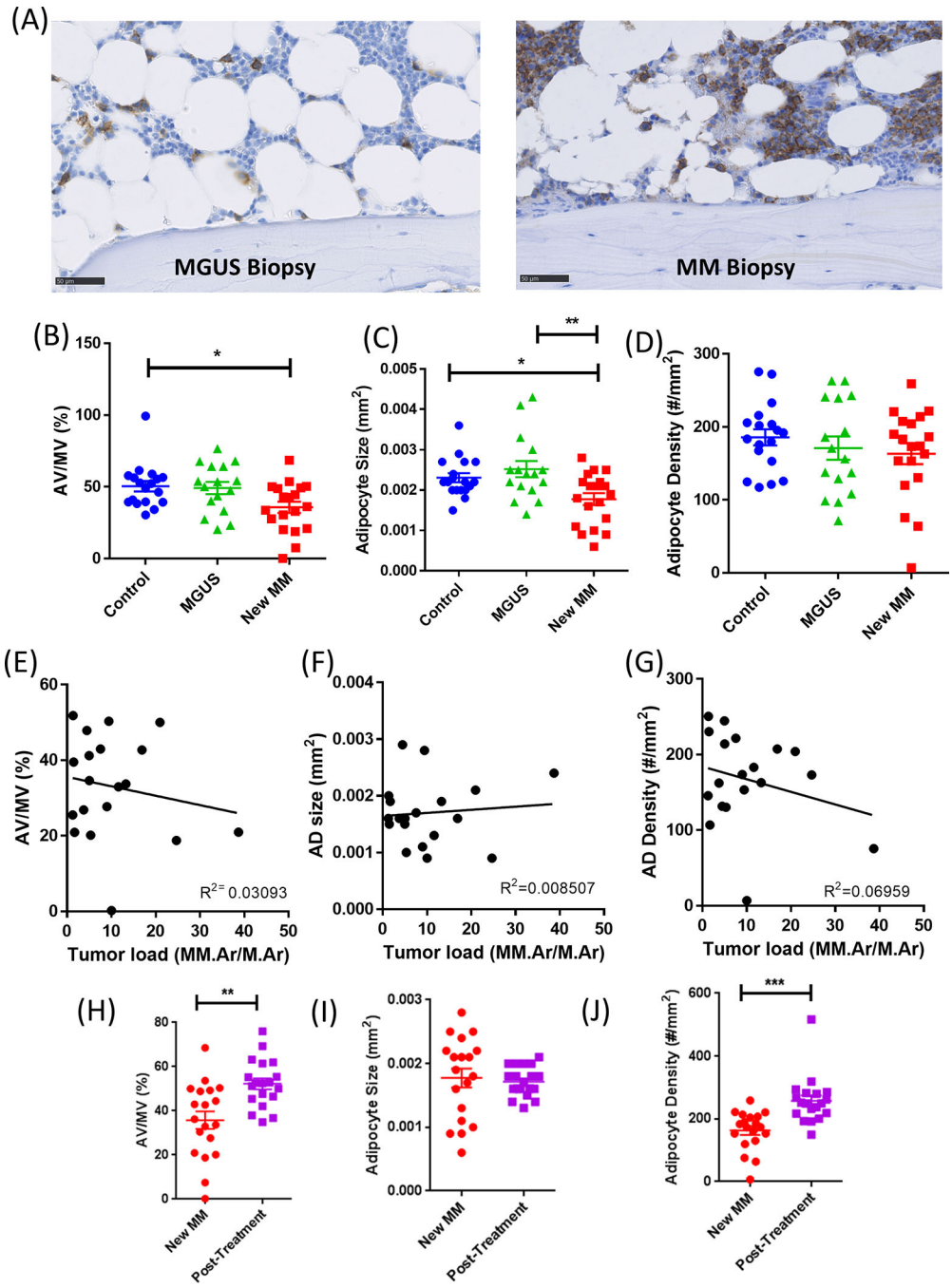

Figure 1. Myeloma cells decrease BMAT in MM patients.

(A) Representative images of CD138 staining of MGUS (left) and MM biopsies (right) using CD138+ IHC and counterstains show that MM cells and BMAds co-localize. Adipocytes indicated as large ghosts (white spaces), myeloma cells indicated by brown stain (40X objective, Scale bar = 50 μm). The BMAT depot was characterized in iliac crest bone specimens from controls (n=18), patients with MGUS (n=16) and MM patients before treatment (New MM, n=19): (B) adipose tissue volume fraction (AV/MV), (C) mean adipocyte size (−29%, P<0.01), and (D) adipocyte density were quantified. Tumor load (MM

tumor area per marrow area, MM.Ar/M.Ar) was not significantly correlated with AV/MV (E), adipocyte size (F), or adipose density (G). Treatment with high-dose melphalan and dexamethasone followed by autologous bone marrow transplantation (n=17) lead to increased AV/MV (H) owing to no significant effect on adipocyte size (I) but a significantly increased adipocyte density (J). *p≤0.05, ** p≤0.005, ***p≤0.001 via two-tailed t-test or one-way ANOVA where applicable.

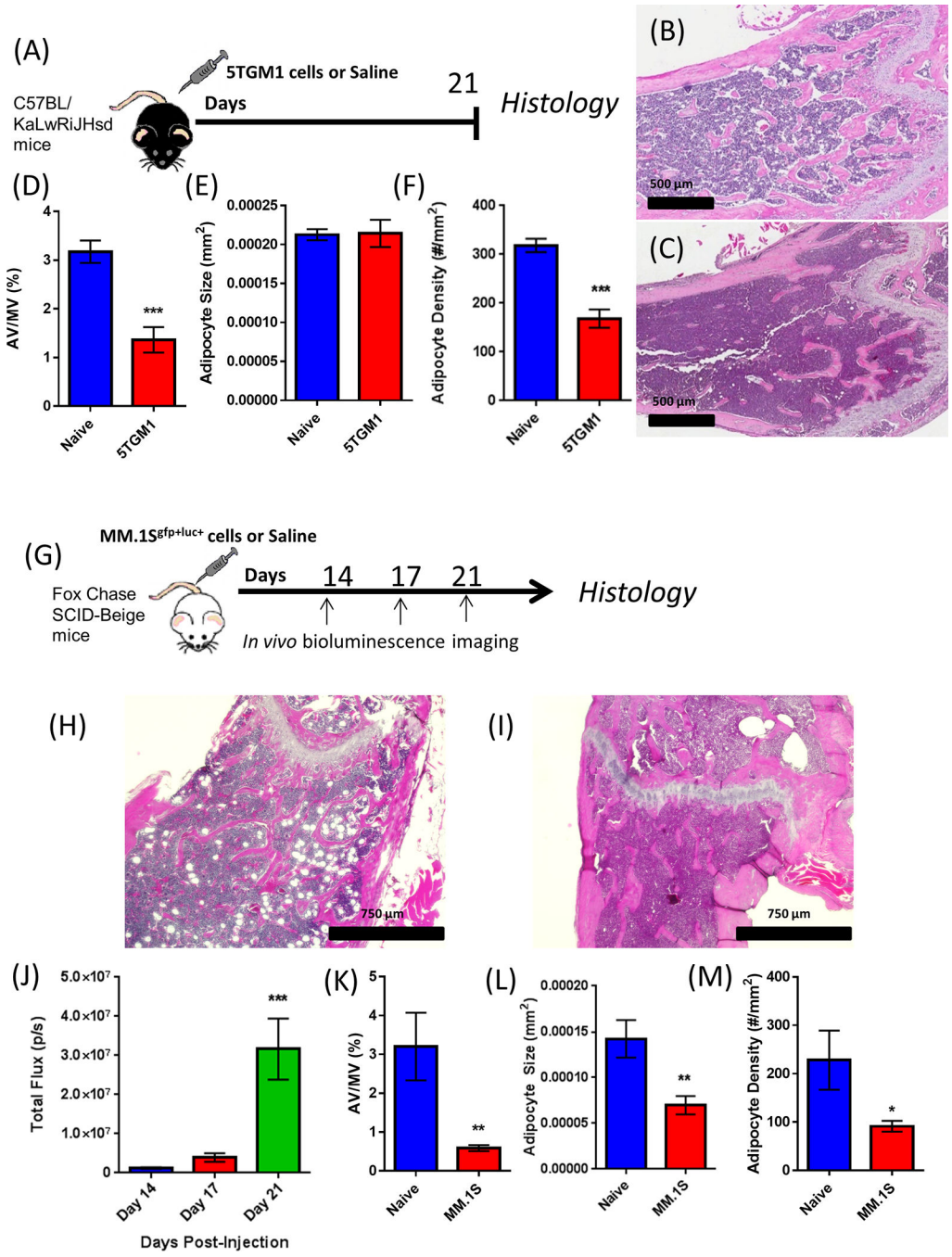

Figure 2. Myeloma cells reduce bone marrow adiposity *in vivo*.

Six to eight-week-old female C57BL/KaLwrRJHsd mice were injected via the tail vein with 0.5 × 10^6 syngeneic 5TGM1-eGFP cells. (A-F) Mice were sacrificed at 21 days following cell inoculation (A) and femora were harvested and fixed in 4% paraformaldehyde for hematoxylin and eosin (H&E) staining from (B) control and (C) tumor-bearing mice. (D) Bone marrow adipocyte volume, (E) adipocyte size, and (F) adipocyte density were quantified utilizing ImageJ; n=5 per group. For the MM.1S model (G-M), 12-week-old female SCID-Beige-MM.1S mice were injected via the tail vein with 5 × 10^6 MM.1S-luc

+/gfp+ cells. Femora were harvested and fixed in 10% neutral buffered formalin prior to (H&E) staining in control (H) and tumor-bearing mice (I) at the endpoint of the survival study. Tumor burden was measured using bioluminescent imaging (BLI) weekly (J) beginning at 2 weeks following cell inoculation until the first mouse reached the predetermined sacrifice point for survival studies. Bone marrow adipocyte volume (K), adipocyte size (L), and adipocyte density (M) were quantified utilizing ImageJ; all femoral sections were imaged with 4X objectives prior to quantification.

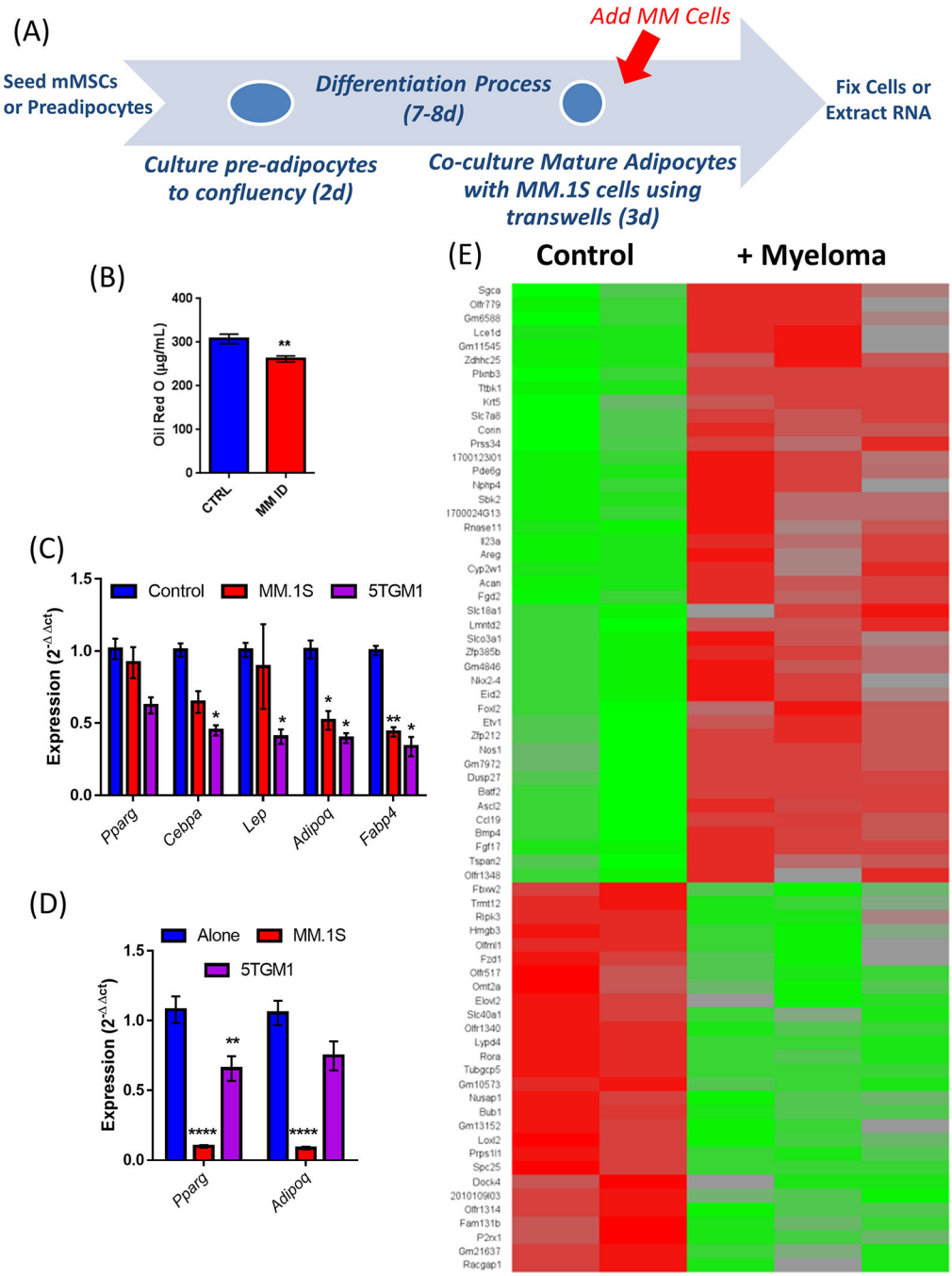

Figure 3. Myeloma-associated adipocytes are phenotypically compromised as reflected by decreased lipid droplet accumulation and aberrant transcriptomes.

(A) Experimental design for experiments with mouse adipocytes. (B) 3T3-L1-derived mouse adipocytes exhibit reduced lipid content (Oil Red-O) after indirect co-culture with MM.1S cells (MM ID) for 72-hours. (C) 3T3-L1 adipocyte gene expression data alone (n=7), or in transwell co-culture with MM.1S (n=9) or 5TGM1 (n=3) MM cells. (D) Mouse bone marrow-derived adipocytes alone (n=23) or in transwell co-culture with MM.1S (n=10) or 5TGM1 (n=10) exhibit lower expression of key adipogenic transcripts. (E) Significant differences in gene expression in mature adipocytes either alone (n=2) or in transwell co-

culture with MM.1S (n=3) for 72-hours as measured via Clariom S mouse microarray. (Red is downregulated (−1.6 fold change), green is upregulated (1.6 fold change)).

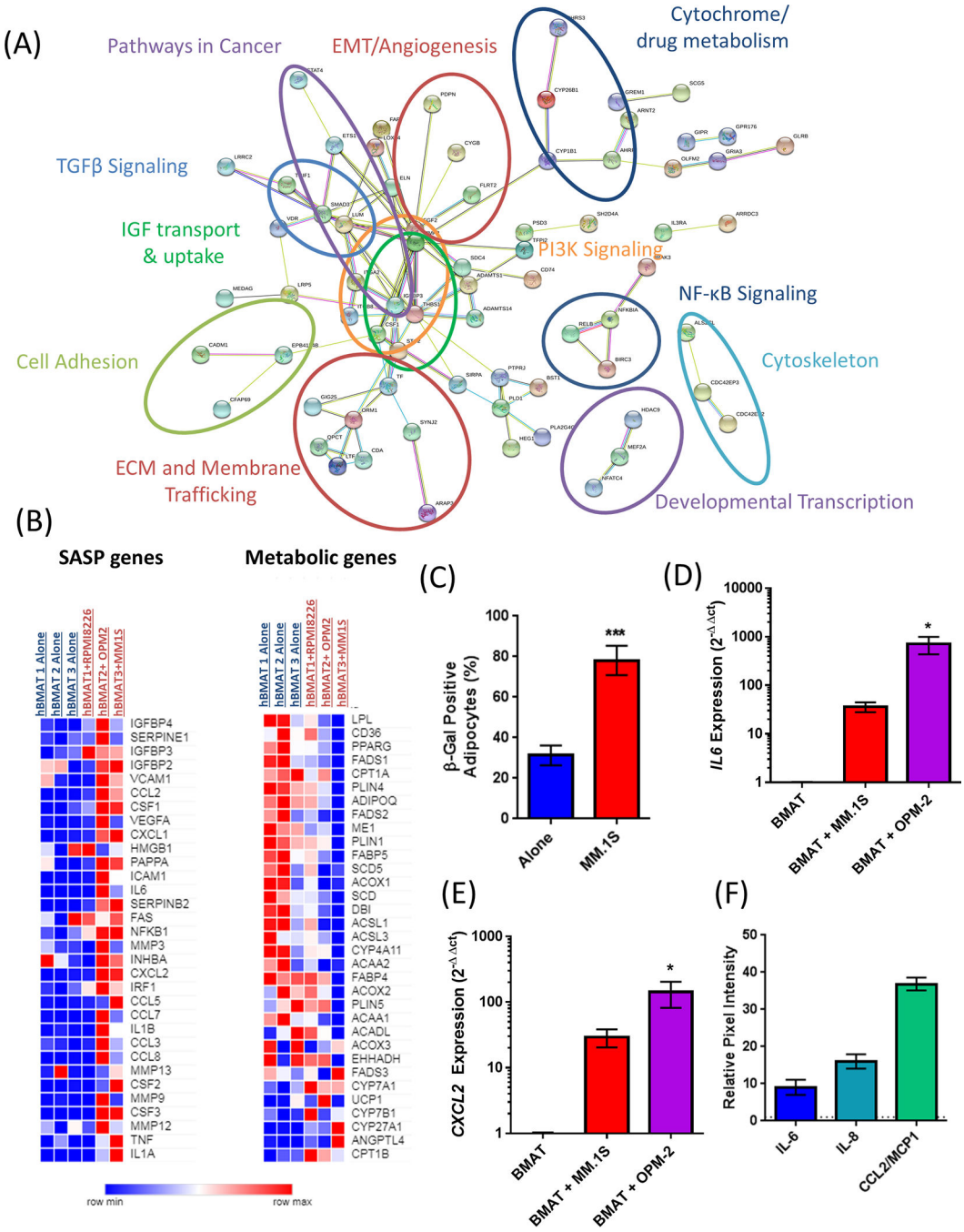

Figure 4. Human BM-MSC-derived adipocytes exhibit aberrant transcripts and display senescence when exposed to myeloma cells.

(A) Genes with expression differences in human BMAT samples exposed to myeloma compared to their controls were selected based on average gene expression fold change (≥2) and significance ($p<0.05$) for DBstring analyses of upregulated genes and networks. (B) Senescence associated secretory phenotype (SASP) genes were examined on an individual basis with expression levels from each sample utilized to build a SASP gene cluster heatmap utilizing the publicly available tool from Morpheus (https://software.broadinstitute.org/morpheus), demonstrating large consistent increases in SASP transcripts in response to MM

cells, specifically the MM.1S and OPM-2 cell lines. Similarly, an adipogenesis cluster was generated utilizing genes incorporated in the KEGG adipogenesis pathway (https://www.genome.jp/kegg-bin/show_pathway?hsa03320) and gene expression levels from each sample reflect decreased adipogenesis in BMAT cultured with MM cells. (C) Quantification of beta-galactosidase (β-gal) positive adipocytes in human BMAds exposed to MM.1S cells for 72 hours. (D) Increased *IL6* and (E) *CXCL2* gene expression was confirmed in three BMAT donors exposed to MM.1S and OPM-2 via qPCR. (F) Elevated cytokines were detected in MM-BMAT co-cultures after 72 hours as detected using cytokine array.

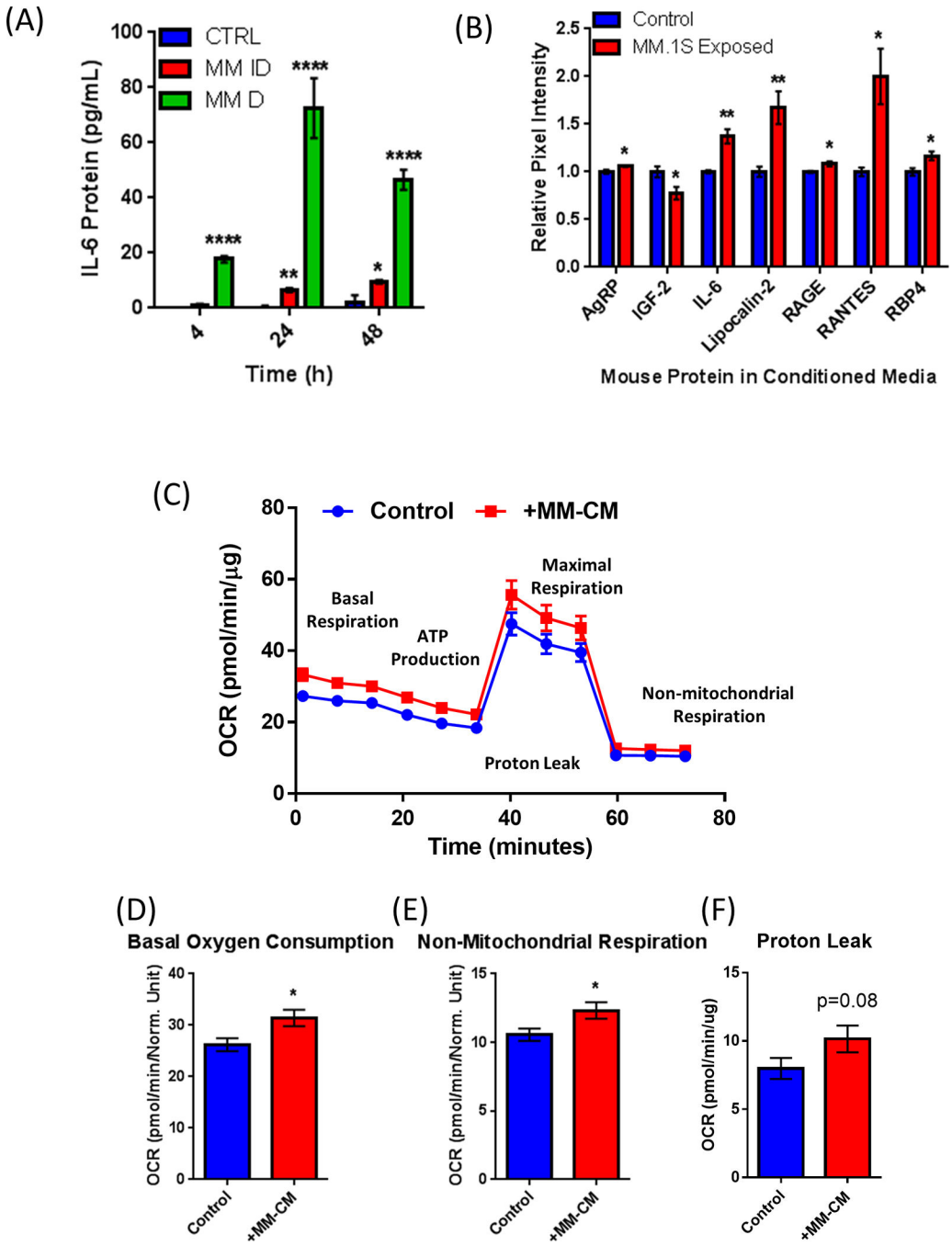

Figure 5. MM-adipocytes exhibit increased IL-6 production and altered cellular metabolism.

(A) Mature 3T3-L1 adipocytes exposed to MM.1S cells via transwell exhibit increased IL-6 secretion after only 4 hours in direct co-culture (MM D), and significant increases in both direct and indirect (MM ID) co-culture systems as detected and quantified by a mouse-specific IL-6 ELISA. (B) Multiple cytokines including IL-6 were significantly increased in the indirect co-culture system, as assessed by mouse adipokine array. (C) Cellular respiration in 3T3-L1 cells following 72-hour exposure to myeloma conditioned media via SeaHorse assay; data collected for approximately 75 minutes at the end of MM-CM

exposure. (D) Basal respiration ($p<0.05$), (E) non-mitochondrial respiration ($p<0.05$), and (F) proton leak (n.s.) are all increased in 3T3-L1 cells exposed to MM.1S-derived soluble factors; data represent three independent experiments and Seahorse experiments used 3T3-L1 cells alone (n=29 wells) or with MM.1S-CM (n=25 wells).

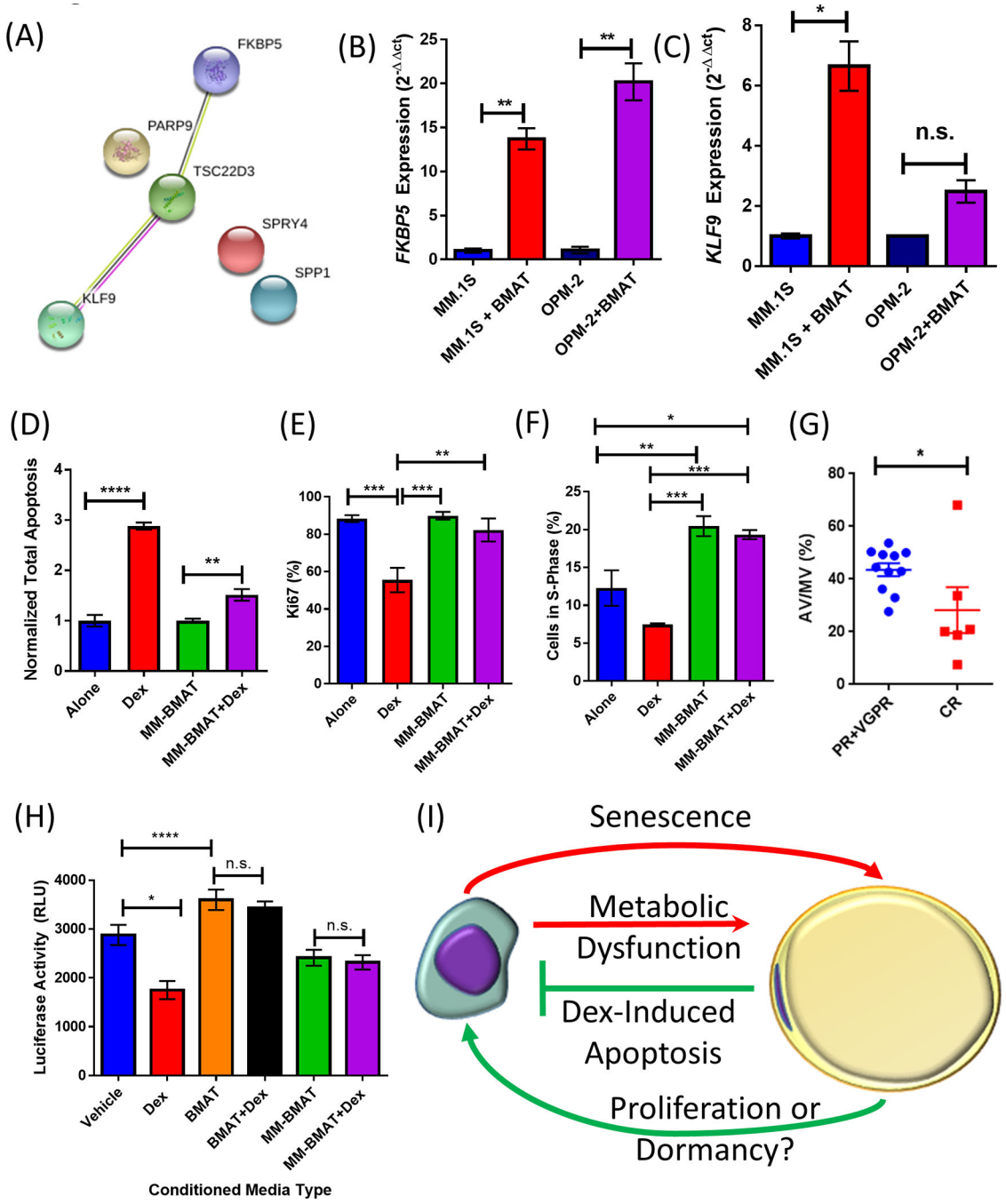

Figure 6. MM-BMAds induce dexamethasone resistance in MM cells *in vitro* and increased adiposity predicts worse outcomes in patients clinically.

(A) STRING analysis of the six commonly upregulated genes in MM cells cultured with BMAT. (B-C) qPCR confirmation of upregulated expression of *FKBP5* and *KLF9* in MM.1S and OPM-2 cells co-cultured with BMAT (n=3 donors). (D) MM.1S cells are resistant to dexamethasone-induced apoptosis (Annexin V, DAPI and (E) proliferation inhibition when co-cultured with BMAT as seen in Ki67 staining, and (F) cell cycle analysis (n=3–6). (G) In primary MM patient bone marrow biopsies, BMAT volume fraction (AV/MV) was analyzed in patients before treatment with high-dose melphalan and dexamethasone followed by

autologous bone marrow transplantation (n=17): MM patients who showed a complete response to treatment (n=6) had significantly lower AV/MV before treatment (−54%, $P<0.05$) compared to patients with partial/very good partial response to treatment (n=11). (H) MM.1S cells were treated with dex for 72 hours in the presence or absence of BMAT CM from naïve or MM-BMAT; bioluminescence was utilized to detect cell number and dex responsiveness (n=7 BMAT donors). (I) Overall schematic of the dynamic relationship between bone marrow adipocytes and myeloma cells.

Table 1.

Top 10 KEGG Pathways significantly altered in 3T3-L1 adipocytes exposed to MM.1S cells.

KEGG Pathway (post-treat)	P-value	Fold Change (FC)
Oxidative phosphorylation	2.06E-07	1.04783
Viral carcinogenesis	1.21E-06	−1.04573
Parkinson’s disease	1.66E-06	1.0448
Ribosome	4.30E-05	1.03017
Cytokine-cytokine receptor interaction	8.90E-05	1.04076
Cell cycle	0.00045873	−1.04318
Spliceosome	0.00053296	−1.0362
MicroRNAs in cancer	0.00080341	−1.04029
Gap junction	0.00117056	−1.05624
Lysine degradation	0.00177668	−1.07781